J Mater Sci: Mater Electron (2011) 22:1473–1478
DOI 10.1007/s10854-011-0332-y

Ni doping effect on electrical conductivity of ZnO nanocrystalline thin films

A. Yildiz · B. Kayhan · B. Yurduguzel · A. P. Rambu · F. Iacomi · S. Simon

Received: 27 January 2011 / Accepted: 3 March 2011 / Published online: 25 March 2011

Abstract The electrical conductivity behavior of undoped and Ni-doped ZnO nanocrystalline thin films prepared by spin-coating method was investigated as a function of temperature. The films were found to have polycrystalline structure. Grain size and the conductivity of the films were found to decrease significantly with increase in Ni concentration. This behavior was well explained by the grain boundary conduction model that takes into account electron trapping in surface states. It was observed that by increasing the Ni-doping level the surface trap density increases and implicitly the conductivity decreases.

1 Introduction

Metal oxide materials like ZnO, SnO_2 and TiO_2 have attracted considerable attention due to their great potential as materials for various applications such as gas sensors [1]. Several reports describing the electrical characteristics of these materials have been published recently [2–6]. The application of gas sensors, in general, requires polycrystalline form of the materials. The size of crystallite has important effect on the gas sensitivity. When the crystallite size is decreased, the surface area increases and then the sensitivity is improved [1]. Therefore, it is desired the nanocrstalline structure for the high sensitivity.

Ni doped ZnO is one of the II-VI diluted magnetic semiconductors (DMSs) [7]. Studies on DMSs have been spurred on by the urge to develop storage device and spin-electronics. The magnetic properties of Ni-doped ZnO thin films present a great interest for many researchers [8, 9]. For films doped with 3–25 at% Ni, ferromagnetism was observed at 2 K. Above 30 K, superparamagnetic behavior was observed [10].

Also, the electrical properties of these materials should be well known for improved performance in such applications. Undoped ZnO exhibits the n-type characteristic due to the native defects such as oxygen vacancies. The electrical conductivity as a function of temperature for Ni-doped ZnO films has been reported [2, 3]. Two different electrical behaviors of Ni-doped ZnO films were reported in literature. According to first behavior, the conductivity increases with increase in Ni concentration. This was explained by the impurity *d*-band splitting model [2]. On the other hand, according to second behavior, the conductivity was found to decrease with increase in Ni concentration [3]. This was explained as follows: oxygen vacancy-related states, which are responsible for high electrical conductivity in undoped ZnO, get compensated by Ni doping, which leads to reduction of conductivity [3]. In spite of extensive investigations, the source of such conductivity behavior is still under debate. There are only a few reports which explain such unusual conductivity behavior for Ni-doped ZnO films as far as we know [2, 3, 11]. Therefore, further

A. Yildiz (✉) · B. Kayhan · B. Yurduguzel
Department of Physics, Faculty of Science and Arts, Ahi Evran University, 40040 Kirsehir, Turkey
e-mail: yildizab@gmail.com

B. Yurduguzel
Programme of Electronic Communication Technology, Kaman Technical Vocational School of Higher Education, Ahi Evran University, 40040 Kirsehir, Turkey

A. P. Rambu · F. Iacomi
Faculty of Physics, Alexandru Ioan Cuza University, 11 Carol I Blvd., 700506 Iasi, Romania

S. Simon
Faculty of Physics & Institute of Interdisciplinary Research in Bio-Nano-Sciences, Babes-Bolyai University, 1 M. Kogalniceanu Street, 400084 Cluj-Napoca, Romania

investigation is necessary to verify exactly the origin of this behavior.

Certainly, there are reported results regarding the properties of Ni-doped ZnO materials obtained by various deposition techniques such as sol–gel method [12], pulsed-electrodeposition-assisted chemical bath deposition method [13], auto-combustion method [14], fast atom beam sputtering technique [15], reactive electron beam evaporation [16], etc.

In order to obtain polycrystalline ZnO:Ni thin films, spin coating method was employed. The spin coating method represents a quite simple and effective way of making thin films with varying its thickness by just controlling parameters such as the time and speed of rotation as well as the viscosity and the density of the coating solution.

In this paper, we present an explanation for the decrease of electrical conductivity with Ni doping in ZnO nanocrystalline thin films, which explicitly takes into account the grain boundary (GB) conduction model.

2 Experimental

Undoped and Ni-doped ZnO thin films were deposited by using spin coating method. The zinc acetate and nickel acetate solutions in N–N-dimethylformamide (2 g metal acetate in 10 ml DMF) were mixed in order to have the Ni/(Zn + Ni) ratios 0.00, 0.04 and 0.06. All the used chemicals were of analytical grade. Microscope glass slides of dimensions 1.6 × 1.6 × 0.1 cm were used as substrates for thin film depositions. The deposition process involved depositing small puddle of a certain solution onto the center of a glass substrate and then spinning the substrate at high speed (3,000 rpm, 60 s). After spinning, the thin films were annealed at 100 °C for 10 min. The procedure was repeated 14 times. Finally, the as-obtained spin-coated films were annealed at 720 K for 1 h in order to evaporate the residual solvent from the films and to obtain oxide nanocrystalline thin films. Thin film thicknesses were measured by using a DEKTAK profilometer and were found to be around 200 nm.

Structural phase identification of the films was carried out by grazing angle X-ray diffraction technique with CuK_α radiation ($\lambda = 1.5418$Å, Shimadzu LabX XRD-6000). Compositional analysis of the thin film surface was conducted using X-ray photoelectron spectroscopy (XPS SPECS PHOIBOS 150 MCD, Al K_α source, 1,486.6 eV). Charge neutralization was used for all samples. Charge referencing was used for all spectra by applying charge correction to the saturated hydrocarbon C 1 s peak at the binding energy of 284.6 eV.

In order to perform the electrical conductivity measurements as a function of temperature, the obtained films were equipped with two parallel thin–film silver electrodes separated by a gap of about 2 mm and the width of each electrode was about 10 mm. The temperature dependence of electrical conductivity was investigated in a temperature range $\Delta T = 300$–400 K.

3 Results and Discussion

The grazing angle X-ray diffraction (GAXRD, $\alpha = 1°$–0.5°, scanning rate of 0.04°/s) patterns of undoped and Ni-doped ZnO films evidenced that films are polycrystalline. The crystalline planes clearly indicate the wurtzite (hexagonal) structure of ZnO [17]. It is significant to note that no traces of the dopant or its respective oxides were observed, indicating a perfect doping of the metals into the ZnO lattice. It was observed that the relative intensity of the main XRD peaks ((100), (002), (101)) changes with Ni doping concentration (Fig. 1, Table 1). If for the undoped sample the intensity of (101) XRD is higher than the intensities of (002) and (100) XRD peaks, by increasing Ni content, the intensities of (100) and (101) XRD peaks become comparable.

It is known that the ionic radius of Zn^{2+} (0.074 nm) is larger than that of Ni^{2+} (0.069 nm) and that when nickel is substituted at the site of zinc, the lattice parameters of zinc

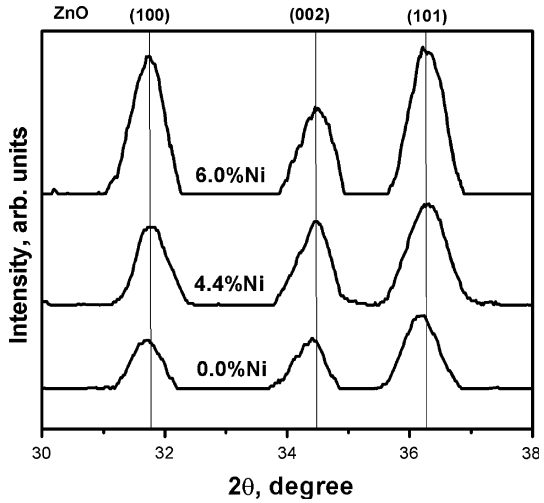

Fig. 1 GAXRD patterns of the films ($\alpha = 1°$ for 0.0% Ni and $\alpha = 0.5°$ for samples 4.4%Ni and 6.0% Ni)

Table 1 Thin film structural characterization

Ni content (at%)	a (nm)	c (nm)	I_{100}/I_{101}	I_{002}/I_{101}	L (nm)
–	0.3253	0.5205	0.66	0.65	19.06
4.4	0.3247	0.5202	0.78	0.79	17.30
6.0	0.3243	0.5170	0.92	0.58	16.96

oxide thin films decreases [18]. In our experiment, unit cell parameter values as determined by using XLAT-Cell Parameter Refinement software (with an accuracy of ±0.0001 nm for "a" parameter and ±0.0005 nm for "c" parameter respectively) indicate a diminution in "a" parameter values confirming that Ni ions entered into ZnO lattice merely by substitution (Table 1).

The broad peaks observed in the XRD pattern are indicative of small particles. The grain sizes (L) of the films were calculated for the main XRD peaks by using Scherrer's formula [19];

$$L = \frac{0.9\lambda}{B\cos\theta} \quad (1)$$

where B is the full-width at half-maximum (FWHM) of (100) diffraction peak, θ is Bragg angle and λ is the X-ray wavelength, respectively. The calculated values of the L are given in Table 1.

The XPS spectra analysis confirmed that the concentration of Ni on the surface of the Ni-doped ZnO thin films is very close to 4.4 at% and 6.0 at%. XPS investigations also evidenced that Zn in all films is in 2+ valence state as the binding energy position of Zn 2p spectra is close to the standard data of zinc oxide (Fig. 2) [20, 21]. Figure 3 shows Ni 2p spectra of Ni-doped ZnO films. The peaks intensity and their width increase with Ni concentration of the films. As shown in Fig. 3, two Ni $2p_{3/2}$ peaks are observed at 854.5 eV and 855.7 eV and a satellite peak at 861.0 eV. These peaks suggest the presence of Ni^{2+} and Ni^{3+} ions in ZnO lattice [22–24].

XPS spectra of O 1s are shown in Fig. 4. The broad and asymmetric nature of the peaks observed for Ni-doped ZnO thin films could be due to various bonds of oxygen in the films. These broad O 1s peaks can be considered as a result of superposition of three XPS peaks having binding energy positions at 529.7 eV, 530.7 eV and 531.9 eV. The first

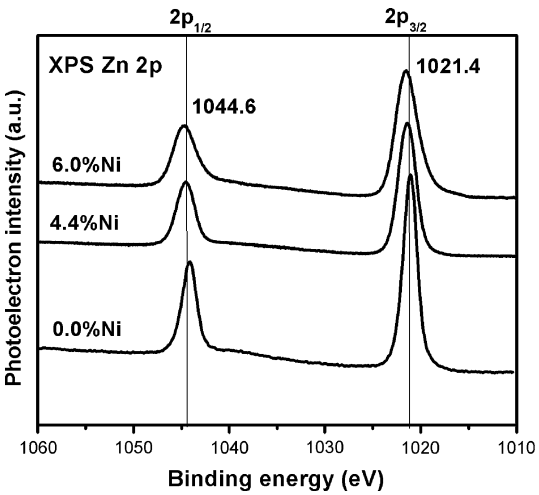

Fig. 2 Zn 2p XPS spectra of Ni-doped ZnO thin films

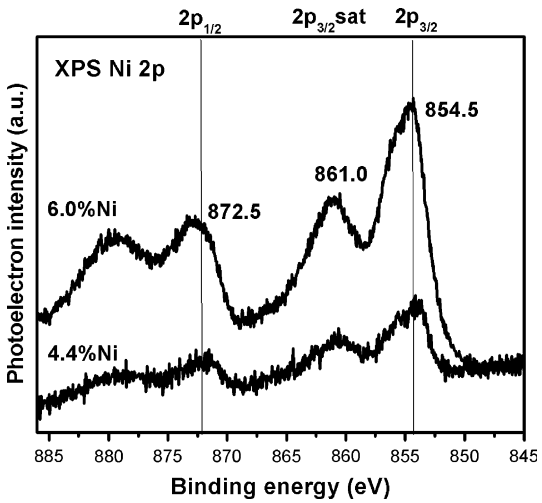

Fig. 3 Ni 2p XPS spectra of Ni-doped ZnO thin films

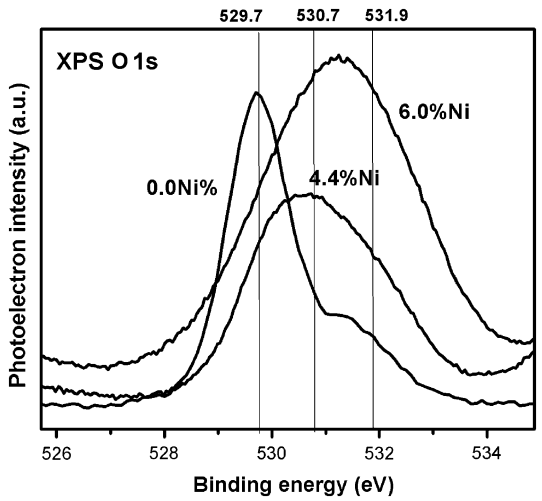

Fig. 4 O 1s XPS spectra of undoped and Ni-doped ZnO thin films

O 1s peak, attributed to O^{2-} ions surrounded by Zn atoms in the wurtzite structure, is the strongest in the undoped ZnO thin film, the second O 1s peak, attributed to O^{2-} ions in oxygen deficient regions within the matrix of ZnO, and the third one, attributed to the presence of loosely bound oxygen species or hydroxyl groups on the surface of the films [15, 25, 26]. The O 1s core level spectra of the doped thin films are dominated by the two components recorded at higher binding energies.

It is evident from the O 1s spectra that defects are increasing with higher percentage of Ni in ZnO [20, 27].

The variation of room temperature conductivity (σ_{RT}) with different Ni concentrations is shown in Fig. 5. The electrical conductivity decreases significantly with the increase in Ni concentration. Inset of Fig. 5 presents the Ni concentration dependent grain size of the films. The grain size decreases as the Ni concentration is increased and this

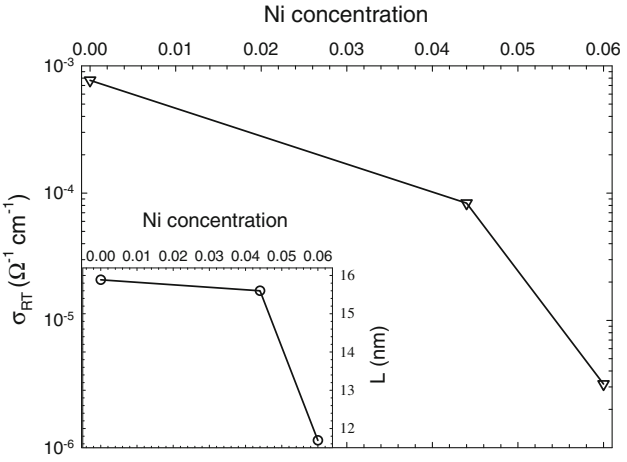

Fig. 5 The variation of thin film room temperature conductivity (σ_{RT}) of the films with different Ni concentrations. Inset presents the Ni concentration dependent grain size of the films

leads to increment in the GB scattering. A similar phenomenon was observed for In doped ZnO films [28]. The smaller grain size of In doped films was attributed to an increased density of nucleation sites due to the incorporation of In [28]. Judging by the change in grain size, it can be concluded that the effect of the GB scattering has to be considered for the investigated films.

Electrical conductivity in polycrystalline materials can proceed through the GB conduction mechanism [29, 30]. Since a polycrystalline film has crystallites joined at their surfaces via grain boundaries (GBs), the boundaries between crystallites play an important role in determining the conductivity of nanocrystalline film. Electron trapping in surface states result in the band bending. This leads to create a potential barrier around the GB. According to the GB model, a decrease in the crystallite size causes an increase in the GB scattering and this leads to a decrease in the electrical conductivity.

In the GB model, the variation of electrical conductivity with temperature depends on whether the grains are fully depleted or partially depleted of charge carriers. Since the undoped ZnO is an n-type material, we can suppose that donor concentration is N_d [31, 32]. When the grains are only partially depleted, the electrical conductivity can be expressed by the following formula [29, 30]:

$$\sigma = \left(\frac{Le^2 n v_c}{k_B T}\right) \exp\left[-\left(\frac{E_C - E_F + e\Phi}{k_B T}\right)\right], \tag{2}$$

where was considered that the barrier energy at boundary, E_b, can be expressed by the relation:

$$E_b = E_C - E_F + e\Phi, \tag{3}$$

and by relation

$$E_b = \frac{L^2 e^2 N_d}{8\varepsilon}, \tag{4}$$

and that

$$v_c = \left(\frac{k_B T}{2\pi m^*}\right)^{1/2}. \tag{5}$$

In Eqs. 2–5 the following notations were used; e, electron charge; k_B, Boltzmann's constant; m^*(=0.3 m_0), effective mass of charge carriers; E_b, barrier energy at boundary; E_C, energy of conduction band minimum; E_F, Fermi level; Φ, grain boundary potential barrier; N_d, donor concentration; ε (=8.5), low frequency dielectric constant.

Figure 6 illustrates the plots of ln $(\sigma T^{1/2})$ vs. $10^3/T$ for the temperatures range 300–400 K for the films. This figure clearly demonstrates that the conductivities decrease monotonically with decrease in temperature, which represents a semiconducting behavior in the whole temperature range. By comparing the curves in Fig. 6, it is noted that there is a remarkable decrease in the conductivity of ZnO films with Ni concentration as compared to the undoped film. The plot of ln $(\sigma T^{1/2})$ vs. $10^3/T$ is analyzed yielding correlation coefficients for least squares fit of about 0.997 for the films, which indicates a satisfactory fit. The values of the E_b are estimated from this plot. The values of E_b are listed in Table 2. The value of E_b increases with increase in Ni concentration. We can also estimate values of the N_d, given in Table 2, from Eq. 4.

One can expect that the activation energies given in Table 2 would related to shallow donor levels which are formed below the conduction band and oxygen vacancy-related states are compensated by Ni doping. And then, it may be anticipated that this compensation leads to drop the Fermi level toward the energy gap, which may cause the

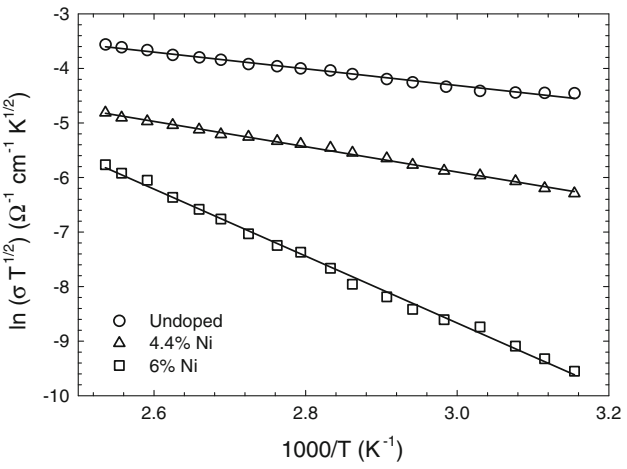

Fig. 6 Temperature dependence of the electrical conductivity plotted as ln $(\sigma T^{1/2})$ vs. $10^3/T$ for the films. *Solid lines* are the best-*fit lines* with Eq. 2

Table 2 Barrier height (E_b), donor concentration (N_d), Debye screening length (L_D), depletion layer width (l_2), and surface trap density (N_t) for the studied films

Ni content (at%)	E_b (eV)	N_d (cm^{-3})	L_D (nm)	l_2 (nm)	N_t (cm^{-2})
–	0.131	1.95×10^{18}	2.88	5.61	3.11×10^{12}
4.4	0.231	3.11×10^{18}	2.28	5.51	4.84×10^{12}
6.0	0.529	1.45×10^{19}	1.05	4.13	1.71×10^{13}

increase in activation energy for the Ni-doped ZnO films. Shallow localized defect states can be also formed with doping, which may contribute to the increase activation energy. On the other hand, the value of the activation energy reaches to 0.53 eV in case of 6% Ni concentration. This energy value is too high for shallow donor levels. Therefore, we ruled out this situation for the investigated films. The conductivity behavior in this study can be explained by the GB conduction model processes common to polycrystalline materials. To further clarify this situation we begin to evaluate some parameters belonging to the GB conduction model. Applicability of the GB conduction model involves many grain boundaries. This effect is examined by evaluation of the L_D in comparison with the L. L_D is given as [30],

$$L_D = \sqrt{k_B T \varepsilon_0 \varepsilon / e^2 N_d}, \tag{6}$$

where ε_0 is the dielectric constant of vacuum. If $L_D < L/2$, potential barriers exist in the GB region due to interface trap states. If, however, L_D is larger than $L/2$, the conduction band becomes flat without the potential barrier. Then carriers are transported without the GB scattering. As seen from Tables 1 and 2, the condition of $L_D < L/2$ is fulfilled for the investigated films, which suggests that the effect of the GB potential barrier on conduction can be taken into account.

Having established the polycrystalline nature of the electrical conductivity, we can determine surface trap density (N_t) at GBs to see how Ni doping affects the electrical conduction. In polycrystalline materials, high density of defects is expected at the GBs, which are often charged with majority carriers. The charged states at the GBs create depleted regions and potential barriers, which provide a resistance for the passage of carriers [29, 30]. There are two cases; either the depletion layer (l_2) extends throughout the grain or only part of the grain is depleted of carriers. In the latter case, the depletion layer width is smaller than the crystallite size ($l_2 < L$) and the surface trap density (N_t) is given as [29]

$$N_t = \frac{(8\varepsilon N_d E_b)^{1/2}}{e} \tag{7}$$

where l_2 is expressed as,

$$l_2 = L_D \sqrt{E_b / k_B T}. \tag{8}$$

The films in this study satisfy the condition $l_2 < L$ (Tables 1 and 2). Utilizing Eq. 7, we can now calculate the values of N_t. The obtained N_t values are in reasonable agreement with the reported values for various polycrystalline materials [29, 30]. As previously mentioned, Ni doping in the films has a drastic effect on the conductivity, changing it by two or three orders of magnitude. When the GB is considered, we explain the observed behavior in the films as follows: as the Ni concentration increases, the grain size decreases, and this leads to an increment in the trapping states at GBs. Trapping states are capable of trapping free carriers, and, as a consequence, more free carriers become immobilized as trapping states increase. Therefore, the conductivity decreases with increase in Ni concentration.

4 Conclusion

The electrical conductivity behavior of the Ni-doped ZnO nanocrystalline thin films prepared by spin-coating method were investigated as a function temperature. XRD and XPS studies evidenced that Ni entered in ZnO lattice as Ni^{2+} and also as Ni^{3+}. Nickel doping determined a diminution in unit cell parameters and grain sizes and an increase in lattice defects. Electrical conductivity of the films decreased significantly with increase in Ni doping in ZnO. A plausible explanation for this behavior includes that takes into account the increase in electron trapping in surface states with Ni doping. The electrical conduction for the investigated films was well inferred within the established framework of grain boundary conduction in polycrystalline materials that have potential barriers at their grain boundaries.

Acknowledgments We are thankful to B.F. Oprea for carrying out XPS measurements. This work was supported by the research projects POSDRU/89/1.5/S/49944 and PN II 12-128/2008 ELOTRANSP.

References

1. H. Meixner, U. Lampe, Sens Act B: Chem. **33**, 198 (1996)
2. S. Singh, N. Rama, M.S.R. Rao, Appl. Phys. Lett. **88**, 222111 (2006)
3. Z. Yin, N. Chen, F. Yang, S. Song, C. Chai, J. Zhong, H. Qian, K. Ibrahim, Solid Stat Commun. **135**, 430 (2005)
4. T. Serin, A. Yildiz, N. Serin, N. Yıldırım, F. Özyurt, M. Kasap, J. Electron. Mater. **39**, 1152 (2010)
5. A. Yildiz, A.A. Alsaç, T. Serin, N. Serin, J. Mater. Sci. doi: 10.1007/s10854-010-0228-2
6. A. Yildiz, F. Iacomi, D. Mardare, J. Appl. Phys. **108**, 083701 (2010)
7. S. Ghosh, K. Mandal, J. Mag. Mag. Mat. **322**, 1979 (2010)

8. C. Jin, R. Aggarwal, W. Wei, S. Nori, D. Kumar, D. Ponarin, A.I. Smirnov, J. Narayan, R.J. Narayan, Metall. Mater. Trans. A doi: 10.1007/s11661-010-0479-9
9. E. Liu, P. Xiao, J.S. Chen, B.C. Lim, L. Li, Curr. Appl. Phys. **8**, 408 (2008)
10. T. Wakano, N. Fujimura, Y. Morinaga, N. Abe, A. Ashida, T. Ito, Physica. C **10**, 260 (2001)
11. X. Liu, F. Lin, L. Sun, W. Cheng, X. Ma, W. Shi, Appl. Phys. Lett. **88**, 062508 (2006)
12. K.T. Kim, G.H. Kim, J.C. Woo, C.I. Kim, Surf. Coat. Technol. **202**, 5650 (2008)
13. X. Huang, G. Li, B. Cao, M. Wang, C. Hao, J. Phys. Chem. C **113**, 4381 (2009)
14. R. Elilarassi, G. Chandrasekaran, Optoelectron. Lett. **6**, 6 (2010)
15. B. Pandey, S. Ghosh, P. Srivastava, D. Kabiraj, T. Shripati, N.P. Lalla, Physica E **41**, 1164 (2009)
16. D.J. Qiua, H.Z. Wu, A.M. Feng, Y.F. Lao, N.B. Chen, T.N. Xu, Appl. Surf. Sci. **222**, 263 (2004)
17. Joint Committee on Powder Diffraction Standards, Powder diffraction file, card no. 36–1451
18. M. Yuonesi, A. Pakdel, Physica B **405**, 2083 (2010)
19. B.D. Cullity, *Elements of X-ray diffraction* (Reading, MA, Addison-Wesley, 1978)
20. B. Pandey, S. Ghosh, P. Srivastava, D. Kabiraj, T. Shripati, N.P. Lalla, Physica E **41**, 1164 (2009)
21. S. Ghosh, P. Srivastava, P.M. Saurav, P. Bharadwaj, D.K. Avasthi, D. Kabiraj, S.M. Shivaprasad, Appl. Phys. A **90**, 765 (2008)
22. A.P. Grosvenor, M.C. Biesinger, RStC Smart, N.S. McIntyre, Surf. Sci. **600**, 1771 (2006)
23. K.T. Kim, G.H. Kim, J.C. Woo, C.I. Kim, Surf. Coat. Techn. **202**, 5650 (2008)
24. E.S. Kumar, S. Venkatesh, M. S. R. Rao1. Appl. Phys. Lett. **96**, 232504 (2010)
25. Y. Jeong, C. Bae, D. Kim, K. Song, K. Woo, H. Shin, G. Cao, J. Moon, ACS Appl. Mater. Interfaces **2**, 611 (2010)
26. M. Chen, X. Wang, Y.H. Yu, Z.L. Pei, X.D. Bai, C. Sun, R.F. Huang, L.S. Wen, Appl. Surf. Sci. **158**, 134 (2000)
27. D.K. Mishra, P. Kumar, S. Kumar, S. Mohapatra, I. Sulania, A. Tripathi, S. Varma, M.K. Sharma, R. Chatterjee, D. Kanjilal, Adv. Sci. Lett. **2**, 324 (2009)
28. B. Szyszka, S. Jager, J. Non-Cryst. Sol. **218**, 74 (1997)
29. J.Y.W. Seto, J Appl Phys **46**, 5247 (1975)
30. J.W. Orton, M.J. Powel, Rep. Prog. Phys. **43**, 1263 (1980)
31. K. Ueda, H. Tabata, T. Kawai, Appl Phys Lett **79**, 988 (2001)
32. M.H. Sukkar, H.L. Tuller, Adv. Ceram. **7**, 71 (1984)